18

Fracturing: Brittleness

CHAPTER PREVIEW

The previous two chapters on mechanical properties described how we test ceramics, their elastic response, and how under certain conditions they can permanently deform. In this chapter we describe why and how ceramics break. The main topics are

- Fracture
- Toughening
- Fatigue

Some of these topics may already be familiar from classes on metals. The exception is probably toughening. Ceramics are not tough. Toughening requires making the material absorb energy during fracture by mechanisms such as local phase transformations, plastic deformation near the crack tip, or crack bridging behind the crack tip. Fracture requires cracks. Fatigue is where crack growth occurs as a result of cyclic loading—even at small loads.

We begin this chapter by showing some of the key equations. The most important work is that of A.A. Griffith, the "father of fracture mechanics." Griffith showed the importance of flaws, which act as stress concentrators. Because it is almost impossible to make ceramics without flaws, they often are the dominant cause of failure. Hence, there is a link between this chapter and Chapter 16.

18.1 IMPORTANCE OF BRITTLENESS

Most ceramics at room temperature are brittle. That is, they fracture with very little plastic deformation. Many archeologists believe that our very existence depended on the brittleness of ceramics, particularly flint. The fracture of flint, like cubic zirconia, diamond, and glass, is termed conchoidal—producing shell-like fracture surfaces. These surfaces are very sharp and were utilized in early stone tools to cut and shape wood and to butcher animals required for food. The hides were used for clothing and were attached to wooden frames to make shelters. Stone tools were necessary for cutting vegetation and cultivating plants, allowing a change from a food-gathering economy to one of food production, which happened around the eighth millennium BCE in southwestern Asia. This revolutionary change from hunting to farming laid the foundation of civilization.

Bulletproof glass, which is a laminate of glass and polycarbonate, is a dramatic illustration of the utilization of brittle fracture. The glass absorbs the energy of the projectile either in elastic changes or ultimately in the creation of new surfaces when it fractures. The polymer provides an additional mechanism for absorption of energy before the projectile exits the final layer. Table 18.1 gives the kinetic energy of several different types of handgun bullets.

The brittle behavior of ceramics is critical to the successful operation of ceramic armor. In addition to brittleness, the basic requirements are that it is:

- Hard
- Lightweight

The first ceramic used in this application was alumina backed with a laminate of fiberglass and polyester resin called "Doron." Boron carbide (B_4C) ceramic armor was developed during the Vietnam War and used in the mid-1960s for both helicopter and infantry armor. It provides the same protection as alumina but with a 20% savings in weight. A quarter inch (0.64-cm) plate of B_4C can stop a 30 caliber armor-piercing projectile (one containing a tungsten carbide core). Boron carbide was being used during the conflict in Iraq. Small arms protective inserts are made of boron carbide. They stop up to a 7.62 mm round with a muzzle velocity of ~850 m/s.

Brittle fracture is used for shaping and machining ceramics after they have been fired. We can modify ceramics to make them machinable. This is called controlled

C.B. Carter and M.G. Norton, *Ceramic Materials: Science and Engineering*,
DOI 10.1007/978-1-4614-3523-5_18,

TABLE 18.1 Kinetic Energy of Handgun Projectiles

Handgun size	*Missile size (g)*	*Missile velocity (m/s)*	*Energy (J)*
0.38	10	243	295
0.22	2.6	305	133
0.45	15	259	503
0.357	10	381	725
9 mm	8	332	440

fracture and is the approach we adopt with machinable glass-ceramics such as Macor (see Chapter 26). Of course, many ceramics already are machinable and can be shaped into intricate and beautiful forms, as illustrated in the carved marble sculpture shown in Figure 18.1.

In many of the applications where we use or would like to use ceramics nowadays, their brittleness can be a serious limitation. Think about:

- Space shuttle tiles are made of silica glass. We need to be concerned about the impact of space debris.
- Radomes are made of fused silica and silicon nitride. They have to be transparent to infrared and radio waves and resist the impact of atmospheric particles.
- Ceramic bearings are used in low-load applications (watch bearings of ruby or sapphire "jewels"); but for high-load and high-speed use, metals are often preferred because ceramics have low fracture toughness.

It is important to remember that metals and polymers can also fracture in a brittle manner, but brittle fracture often occurs only at temperatures below room temperature.

FIGURE 18.1. Marble sculpture in a fountain outside the Pantheon in Rome.

18.2 THEORETICAL STRENGTH: OROWAN EQUATION

We consider brittle fracture at the atomic level where we are separating two planes of atoms, as shown in Figure 18.2A. In many crystalline materials, fracture occurs along crystallographic planes that are relatively densely packed. These planes are known as cleavage planes. In MgO, {100} is the cleavage plane. [It is interesting that {111} is the growth plane for MgO and that fluorite is exactly the opposite!] In glasses and in some crystals (diamond and cubic zirconia, for example), fracture is noncrystallographic.

Figure 18.2B shows a plot of stress versus distance. Note that we are using X for distance (rather than r, as we did in Chapter 3) because we are now thinking about planes of atoms rather than individual atoms. The curve

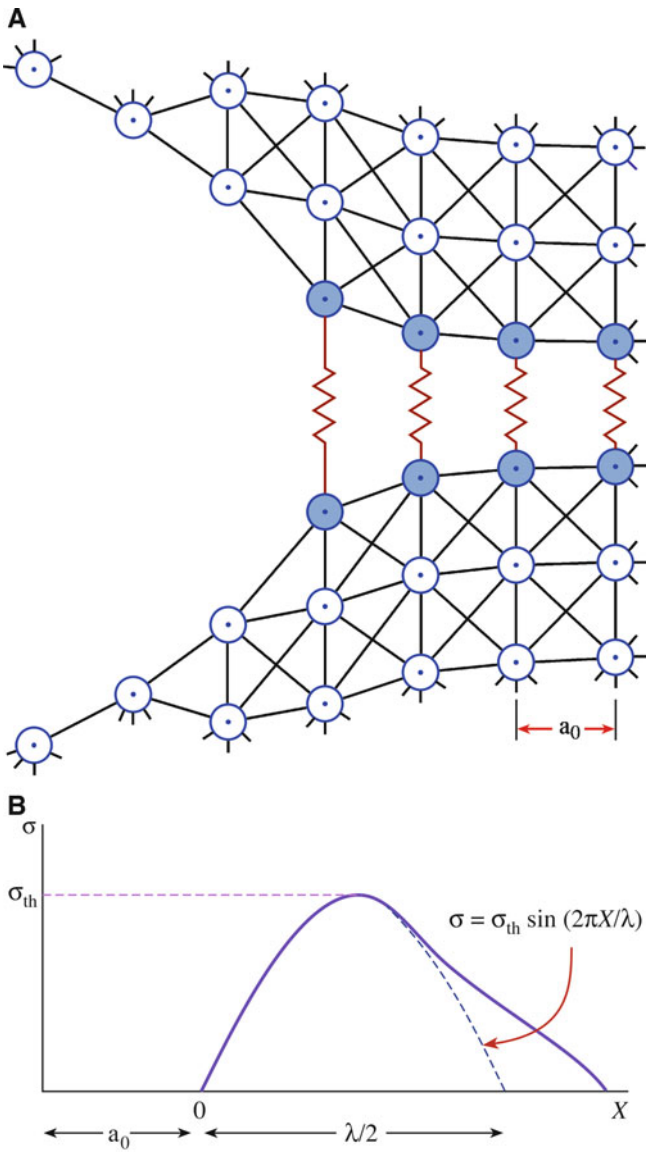

FIGURE 18.2. (A) Model of a crack tip. The interplanar spacing is a_0. (B) Stress versus distance plot.

is the same; it is only the notation that changes. If a stress is applied that exceeds the theoretical strength, σ_{th}, the ceramic fractures. This is the strength of the ceramic if there is no plastic deformation and there are no defects. It is "theoretical" because we can rarely, if ever, achieve it. We would like to be able to obtain an expression for σ_{th}, and there are several different approaches we can use. The one we have selected is simple, works well, and gives values similar to those obtained by more complex methods.

The part of the σ–X curve near the equilibrium interplanar spacing, a_o, can be approximated as being sinusoidal, and we can write:

$$\sigma = \sigma_{th}\sin(2\pi x/\lambda) \tag{18.1}$$

where x is the displacement of the planes beyond their equilibrium value, and λ is the wavelength of the sine wave.

Two new surfaces are created during fracture—the fracture surfaces. They have a total energy 2γ, which must be equal to the work required to separate the two planes of atoms (i.e., it is the area under the curve or the integral of equation 18.1 between 0 and $\lambda/2$):

$$2\gamma = \int_{o}^{\lambda/2} \sigma_{th}\sin(2\pi x/\lambda)dx = \lambda\sigma_{th}/\pi \tag{18.2}$$

Rearranging equation 18.2 gives:

$$\sigma_{th} = 2\pi\gamma/\lambda \tag{18.3}$$

For low stresses, the material is elastic, Hooke's law is obeyed, and we can write the Young's modulus as:

$$\mathcal{E} = \sigma a_0/x \tag{18.4}$$

and

$$d\sigma/dx = \mathcal{E}/a_0 \tag{18.5}$$

For small displacements, we can make the approximation $\sin x \sim x$, and from equation 18.1 we can write:

$$d\sigma/dx = 2\pi\sigma_{th}/\lambda \tag{18.6}$$

Combining equations 18.5 and 18.6 gives:

$$2\pi\sigma_{th}/\lambda = \mathcal{E}/a_0 \tag{18.7}$$

By substitution of equation 18.3, we get the Orowan equation:

$$\sigma_{th} = (\mathcal{E}\gamma/a_0)^{1/2} \tag{18.8}$$

Theoretical strength thus depends on:

- Surface energy
- Young's modulus
- Lattice spacing

Putting in reasonable values for γ (see Chapter 13) and a_0, we find that $\sigma_{th} \approx \mathcal{E}/5$ to $\mathcal{E}/10$. This is a useful relationship to remember. Values of σ_{th} for some materials calculated using the Orowan equation are given in Table 18.2. These values are possible only in very special forms, such as silica fibers with pristine surfaces. Whiskers and fibers of sapphire and silicon carbide have been made with measured strengths of about $\sigma_{th}/2$ (Table 18.3).

For most polycrystalline ceramics, measured strengths are in the range of $\mathcal{E}/100$ to $\mathcal{E}/1000$ or even less. The question is: why is there such a large discrepancy between theoretical and measured strengths? The reason is the presence of preexisting cracks on the surface or inside the ceramic and the sharp corners that may be introduced during processing. The presence of cracks does not mean that samples fracture spontaneously: our teeth are full of cracks.

18.3 EFFECT OF FLAWS: GRIFFITH EQUATION

To explain the discrepancy between theoretical strength predicted by equation 18.8 and experimental data, Griffith (1920) suggested that preexisting flaws in the materials act to concentrate stress. Figure 18.3 shows data obtained by

TABLE 18.2 Values of Theoretical Strength

Material	*Direction*	$\mathcal{E}$*(GPa)*	γ *(J/m^2)*	σ_{th} *(GPa)*
α-Fe	<111>	132	2	30
Si	<111>	188	1.2	32
NaCl	<100>	44	0.25	6.3
MgO	<100>	245	1.2	37
Al_2O_3	<0001>	460	1	46

TABLE 18.3 Comparison of Theoretical Strength and Actual Strength

Material	$\mathcal{E}$*(GPa)*	*Estimated theoretical strength (GPa)*	*Measured strength of fibers (GPa)*	*Measured strength of polycrystalline specimen (GPa)*
Al_2O_3	380	38	16	0.4
SiC	440	44	21	0.7

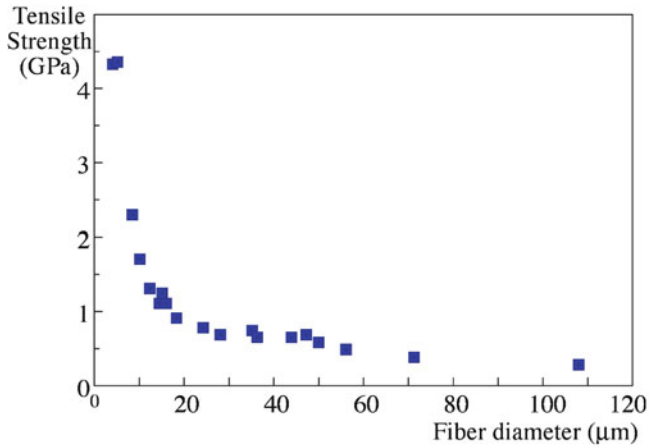

FIGURE 18.3. Tensile strength of glass fiber as a function of fiber diameter.

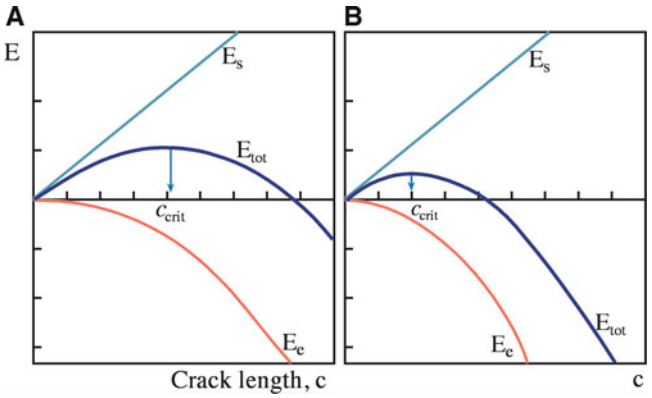

FIGURE 18.4. Plots of energy versus crack length. U_{tot} is the sum of U_s and U_e. The right plot corresponds to a greater applied stress (on this scale, the stress is greater by $\sqrt{2}$, and c_{crit} is correspondingly reduced by a factor of 2).

Griffith for the tensile strength of glass fibers as a function of their diameter. As the fibers get smaller, the probability of having a crack decreases and the size of the largest crack also decreases. Consequently, they get stronger. This is the basis of the "weak link" approach adopted in Weibull statistics that we described in Chapter 16. Hence, there is a direct relationship between flaws and the probability of failure.

Griffith's approach is an energy balance: a crack propagates when the additional energy created by the formation of the fracture surfaces, E_s, is offset by a decrease in the stored elastic energy, E_e, in the stretched bonds (this is the area under the stress–strain curve). The Griffith energy balance condition can be expressed as

$$\frac{dE_e}{dc} = \frac{dE_s}{dc} \tag{18.9}$$

Note that we are using E for energy to avoid any confusion with Young's modulus ($\mathcal{E}$). The elastic energy term is:

$$E_e = \pi\sigma^2 c^2/\mathcal{E} \tag{18.10}$$

The surface energy term is

$$E_s = 4c\gamma \tag{18.11}$$

Because E_s scales linearly with c and E_e scales quadratically with c, there is a maximum in the total energy E_{tot} of the system, which corresponds to the critical crack size, c_{crit}. This balance can be represented graphically, as shown in Figure 18.4.

- A crack smaller than c_{crit} is stable; the surface energy dominates.

SCRIBING

A simple illustration of the effect of surface flaws is the ease with which a sheet of glass can be 'cut' after light scribing using a diamond tip.

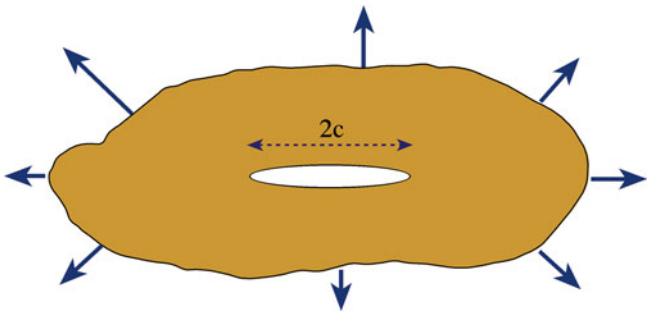

FIGURE 18.5. "Griffith" crack of length 2c.

- A crack larger than c_{crit} is unstable; the released strain energy dominates.

For an atomically sharp crack of length $2c$, as illustrated in Figure 18.5, the energy balance approach shows that:

$$\sigma_f = (2\mathcal{E}\gamma/\pi c)^{1/2} \tag{18.12}$$

Equation 18.12 is often called the Griffith equation and shows that fracture stress depends on:

- Young's modulus (a property of the material)
- Surface energy (a property of the material)
- Crack length

Griffith confirmed this equation using experimental data on glass, as shown in Figure 18.6. Although the energy balance approach works well, kinetic effects may also be present during fracture, as demonstrated for the fracture of mica flake.

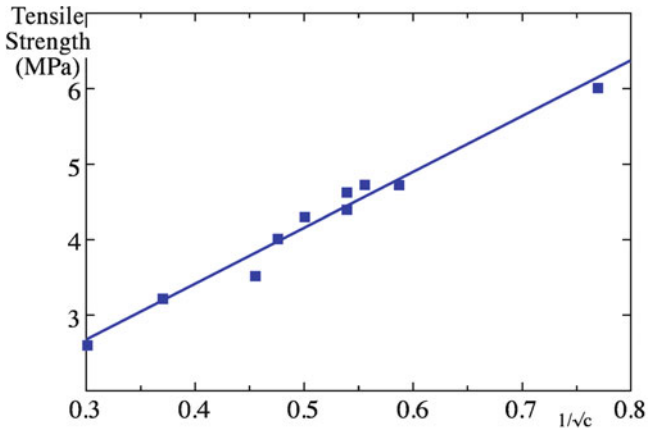

FIGURE 18.6. Verification of equation 18.12. Tensile strength of glass as a function of crack length.

18.4 CRACK TIP: INGLIS EQUATION

In our discussions of fracture, so far we have assumed that the crack looks much like that shown in Figure 18.2a. The crack separates planes of atoms, is atomically sharp, and the only deformation is elastic and ahead of the crack tip. This is the situation encountered in many ceramics at room temperature.

For the geometry in Figure 18.5, the maximum tensile stress at the crack tip is:

$$\sigma_m = 2\sigma(c/\rho)^{1/2} \tag{18.13}$$

where ρ is the crack tip radius. The ratio σ_m/σ is called the stress concentration factor. As an illustration of how big the stress concentration factor can be, we consider an example of a ceramic with a flaw size c of 50 μm. The stress concentration at the crack tip is about 1,200.

Al ALLOYS
Fracture toughness ~40 MPa/m^2

For fracture to occur in an ideal brittle material, the maximum stress must reach the theoretical strength of the material to provide a mechanism for fracture (i.e., $\sigma_m = \sigma_{th}$). If we set the applied stress (σ) equal to the fracture stress (σ_f), we obtain:

$$\sigma_f = \left(\frac{\mathcal{E}\gamma}{4c}\frac{\rho}{a_0}\right)^{\frac{1}{2}} \tag{18.14}$$

From equation 18.14, you can see why sharp cracks are so deleterious to the strength of ceramics. For metals, there is often a plastic zone ahead of the crack tip that is due to dislocation motion. This leads to blunting of the crack tip and a corresponding decrease in stress concentration.

A crack in a brittle material passes between adjacent planes of atoms, and a reasonable estimate for the tip radius is half the atomic spacing. Therefore, we can simplify equation 18.14:

$$\sigma_f = (\mathcal{E}\gamma/8c)^{1/2} \tag{18.15}$$

The fracture process, although not far from ideal in ceramics, can be quite complex. Real cracks differ from those assumed in the model in that there is often no distinct crack edge. There are attractive interactions between atoms on opposite sides of the crack when the spacing is quite small.

18.5 STRESS INTENSITY FACTOR

We introduced the stress intensity factors in Chapter 16. These are a combination of c and σ for different loading geometries with respect to crack position.

The most important geometry for ceramics is mode I, the opening mode. The mode I stress intensity factor is

$$K_I = \sigma Y\sqrt{c} \tag{18.16}$$

where Y is a dimensionless term that depends on crack configuration and loading geometry. For a simple interior crack of length $2c$ and tensile loading, $Y = \sqrt{\pi}$ (this is the original geometry considered by Griffith); for a surface crack under similar loading, $Y = \sqrt{(\pi/2)}$.

The critical stress intensity factor for mode I loading, K_{Ic}, at which the crack propagates and leads to fracture is known as the fracture toughness (sometimes denoted as T). Table 18.4 lists some values for ceramics. You can see that the values are generally low, and a significant amount of research has been undertaken over the last four decades to increase K_{Ic}. We look at some of the approaches that have been used a little later in this chapter.

If the material is not perfectly brittle (i.e., there are energy-dissipating mechanisms in addition to the creation of new surfaces), then we introduce a term G_c, which is an energy (its units are J/m^2) representing crack extension by all the available processes. You may find G_c referred to as total work of fracture, crack extension force, and the strain energy release rate.

For plane stress (the sample is a thin plate):

$$K_{Ic} = \sqrt{(\mathcal{E}G_c)} \tag{18.17}$$

TABLE 18.4 Fracture Toughness for Several Ceramics

Ceramic	*K_{Ic} (MPa/m^2)*
Al_2O_3	2.0–6.0
Al_2O_3 (single crystal, 10–12)	2.2
Al_2O_3 (single crystal, 0001)	>6.0
MgO	2.5
$MgAl_2O_4$	1.9–2.4
Mullite (fully dense)	2.0–4.0
ThO_2	1.6
Y_2O_3	1.5
ZrO_2 (cubic)	3.0–3.6
ZrO_2 (partially stabilized)	3.0–15.0
SiC (hot pressed)	3.0–6.0
SiC (single crystal)	3.7
Si_3N_4 (hot pressed)	3.0–10.0
TiC	3.0–5.0
WC	6.0–20.0
CaF_2	0.80
KCl (single crystal)	~0.35
MgF_2	1.00
SrF_2	1.00
Aluminosilicate glass (Corning 1720)	0.96
Borosilicate glass (Corning 7740)	0.75
LAS (glass-ceramic)	2.00
Silica (fused)	0.80
Silica (96%)	0.70
Soda-lime silica glass	0.82

For plane strain (the sample is a thick block):

$$K_{\mathrm{Ic}} = \sqrt{\frac{\mathcal{E}G}{(1-\upsilon^2)}} \tag{18.18}$$

When fracture occurs we can write:

$$G_{\mathrm{c}} = dE_{\mathrm{s}}/dc = R \tag{18.19}$$

Where R is the crack resistance of the material and is called the crack resistance "force." The material fractures when $G_c = R$; that is, the crack extension force is equal to the crack resistance force. If the fracture is entirely brittle, the energy is required only to create new surfaces; then $R = 2\gamma$. (Note: the surface energy term used here differs from that in equation 18.11 by a factor of two because G_c is associated with a single crack tip.)

Table 18.5 compares some measured values of G_c to some theoretical values based on surface energies. You can see that for MgO the two values are in good agreement. This is not the case for the metal alloys.

18.6 R CURVES

The crack resistance R is related to fracture toughness as we just described. It was assumed that R and T are independent of crack length, but this is not necessarily so. The R curve, which is a plot of fracture toughness versus crack length, relates the crack resistance to crack length, as shown in Figure 18.7. The fracture toughness increases as the crack grows. We can explain the shape of these curves by considering what happens in the wake of the crack. If there is a mechanism that bridges the crack, then the energy required for crack propagation increases. There are several mechanisms that can be envisaged, for example, a phase transformation associated with crack propagation or ligaments that bridge the crack after the crack tip has passed. Both mechanisms are described when we discuss how we actually try to toughen ceramics.

TABLE 18.5 Theoretical and Measured Values of G_c for Some Materials

Material	*Theoretical $G_c = 2\gamma$ (N/m)*	*Measured G_c (N/m)*
Glass	3.5	14
Plexiglass	11.4	480
MgO	14.9	17.5
High-strength steel	22.8	53,000
High-strength aluminum	7.0	17,000
High-strength titanium	10.5	105,000

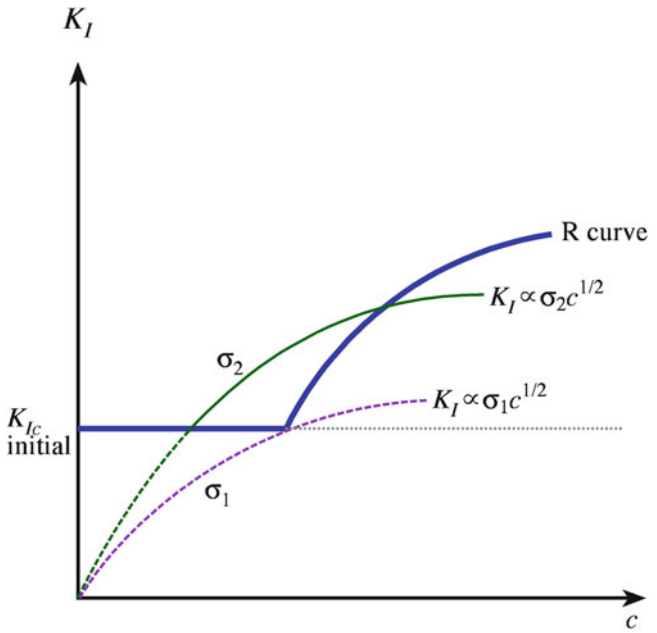

FIGURE 18.7. A material showing R curve behavior (*bold curve*) exhibits a region with stable crack growth and flaw-tolerant behavior. The lighter curves, σ_1 and σ_2, represent typical Griffith behavior.

Eventually, a plateau is reached beyond which fracture toughness does not increase. This is the steady-state condition. The implications for ceramics that show R curve behavior are:

- Strength degradation less dependent on flaw size (illustrated in Figure 18.8).
- Increased reliability. There is a region where the strength is insensitive to crack size.
- Decreased fatigue resistance.
- Better thermal shock resistance.

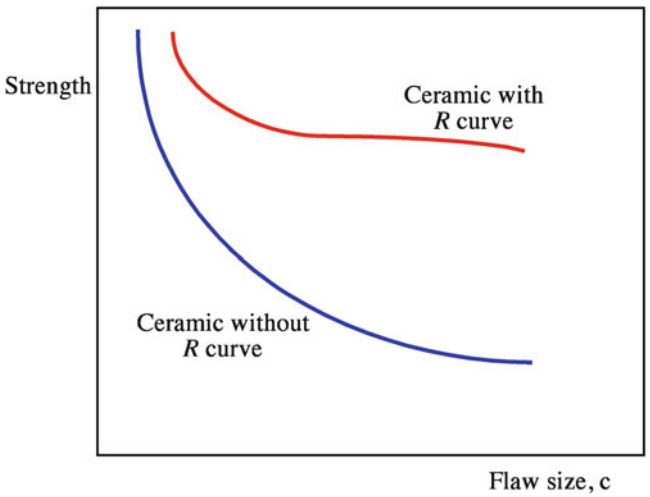

FIGURE 18.8. Effect of R curve behavior on strength. There is a region where the strength is insensitive to flaw size.

18.7 FATIGUE AND STRESS CORROSION CRACKING

The cracks that we have been describing so far lead to rapid fracture. We call them "critical cracks." Ceramics may contain many other cracks, called "subcritical cracks," that can lead to time-dependent fracture. Static fatigue, also known as stress rupture, is where subcritical cracks grow under an applied load. Failure occurs gradually and is often unexpected; it may occur after a component has been in service for many years.

CORROSION & FAILURE

The corrosion rate of silica glass in water is 10^{-17} m/s.
The rate of stress corrosion cracking (SCC) is 10^{-3} m/s.

The slow growth of cracks is often the result of a combination of stress and corrosion. This is the field of stress corrosion cracking (SCC), which is important in metals such as gold jewelry alloys and many ceramics. Figure 18.9 shows experimentally measured crack velocities in soda-lime glass tested in nitrogen of varying relative humidity. We can identify three distinct regions.

Region I: crack growth is sensitive to K_I and follows a relationship of the form:

$$v = A^* \exp \alpha K_I \qquad (18.20)$$

where A^* and α are fitting parameters. From an engineering point of view this is the most important region.
Region II: crack growth independent of K_I
Region III: very rapid crack growth leading to fracture

For many materials there exists a threshold value of K_I, below which the crack does not grow. This value is not seen in Figure 18.9 because of the experimental difficulties of measuring very small values of crack velocity.

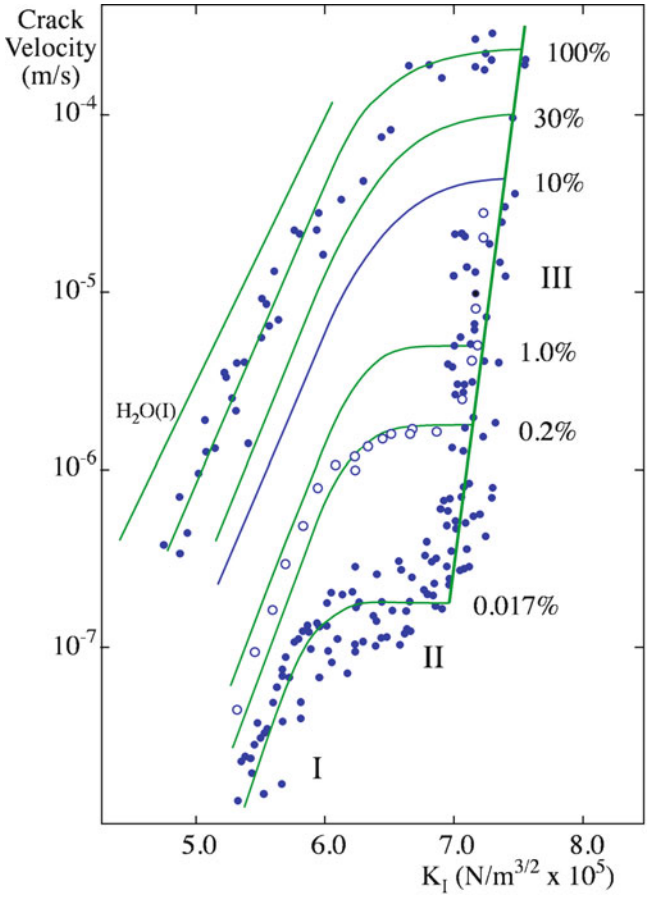

FIGURE 18.9. Crack velocity in soda-lime glass as a function of K_I, the stress intensity factor. The percentages indicate the relative humidity, and the Roman numerals indicate the three regions of crack propagation.

Figure 18.10 illustrates the process that is happening at the crack tip. The corresponding reaction, which involves breaking of Si-O bonds, is:

$$Si - O - Si + H_2O \rightarrow 2Si - OH$$

Other small polar molecules, such as methanol (CH_4OH) and ammonia (NH_3), can promote SCC in glass. The main requirement is that they are small enough to fit into the crack (<0.3 nm).

Ceramics can also fail by cyclic fatigue. The mechanisms are complicated and not well understood. Fatigue failure in metals is pervasive and due to dislocation motion.

Because fatigue is due to propagation of cracks, it is related to K. During a fatigue cycle, K varies, so what we are actually interested in is ΔK, the difference between K at maximum load (K_{max}) and K at minimum load (K_{min}).

$$\Delta K = K_{max} - K_{min} \qquad (18.21)$$

Figure 18.11A shows a log–log plot of the crack growth rate (dc/dN), where N (the number of cycles—hence the odd units) is plotted against ΔK. We can identify three distinct regions.

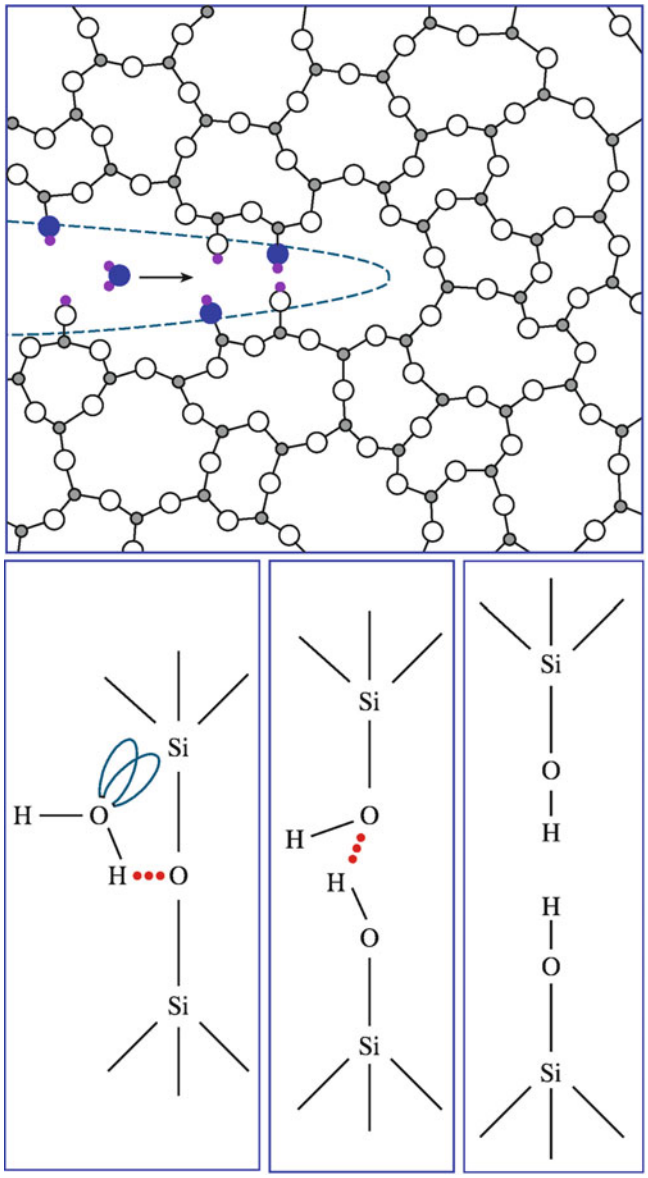

FIGURE 18.10. Environmental effects at the crack tip. A water molecule diffuses to the crack tip, chemisorbs, and rotates such that the lone pairs on the oxygen are aligned with the unoccupied electron orbitals of the Si atom.

Region I: the lower limit to the curve ΔK_T is the threshold stress intensity factor range for crack growth. In this range, crack growth with cyclic loading is negligible, if indeed it occurs at all.

Region II: the plot is linear, and the crack growth rate can be described by the following equation (sometimes called the Paris-Erdogan equation)

$$dc/dN = B(\Delta K)^q \qquad (18.22)$$

where B and q are materials constants that are determined empirically.

Region III: at high ΔK values, crack growth is very rapid; and fracture would be characteristic of normal static failure.

Figure 18.11B shows examples of cyclic fatigue plots for several ceramics. The curves are linear and very steep, implying a high value of q in equation 18.22 and that fracture is rapid. The fatigue fracture we see in metals is rare in ceramics.

18.8 FAILURE AND FRACTOGRAPHY

Here we discuss the appearance of different surfaces formed when a ceramic fractures. This is the topic of fractography and is always a postmortem analysis. Fractography is used not only to determine the failure mechanism but also the origin of fracture. Examples of where fractography is used include:

- Dentistry (e.g., examination of teeth to improve survivability)
- Liability cases (e.g., hip implants to determine who's to blame)
- Disasters (e.g., space shuttle tiles to make sure problem doesn't recur)

Figure 18.12 illustrates two different crack paths through a material. In Figure 18.12A, the crack passes between grains, and fracture is termed intergranular. Intergranular fracture is most likely when the grain boundaries are weak. A striking example of intergranular fracture is shown in Figure 18.13A. The ceramic is AlN that was prepared by sintering, with Y_2O_3 added as a sintering aid. The individual grains, which are faceted, can be clearly seen in the scanning electron microscopy (SEM) image.

In transgranular (or cleavage) fracture, the crack passes through the grains, as illustrated in Figure 18.12B. The fracture surface may be smooth or show steps, which form as the crack front moves from one plane to another. Figure 18.13B shows transgranular fracture in polycrystalline SiC. In conchoidal fracture, there are no distinct cleavage planes. As we mentioned earlier, conchoidal fracture occurs in flint, cubic zirconia, diamond, and glass.

When fracture surfaces are examined, in addition to determining the failure mechanism we also are often interested in the origin of fracture, which might help identify the cause. By reassembling the pieces and looking for where cracks come together, as illustrated in Figure 18.14, it is possible to determine crack initiation sites. They may be associated with flaws (e.g., pores or inclusions) introduced during processing.

The extent of crack branching provides information about the amount of energy associated with crack propagation. There is more branching if the applied stresses are large or if there are large residual stresses that are released as the crack advances. The latter principle is utilized in tempered glass. Extensive crack branching occurs, causing the glass to eventually break into many small pieces.

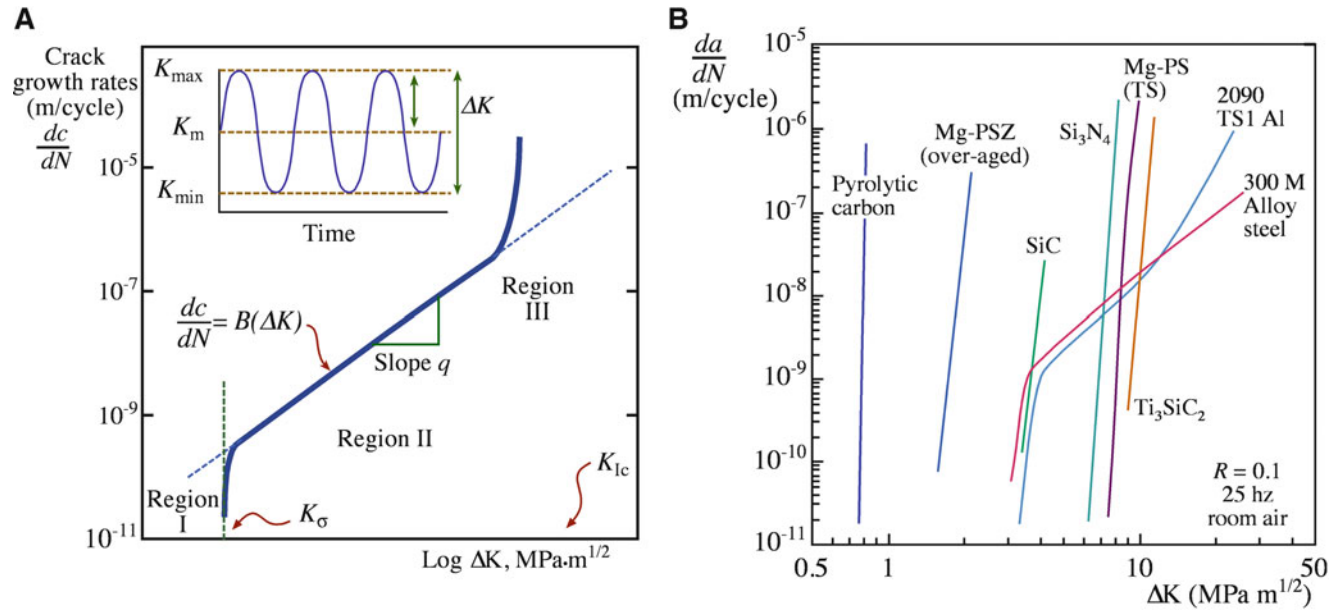

FIGURE 18.11. (A) Log–log plot of crack growth rate dc/dN versus K (defined in the inset). (B) Cyclic-fatigue crack growth rates for several ceramics and metal alloys as a function of applied stress intensity range, ΔK.

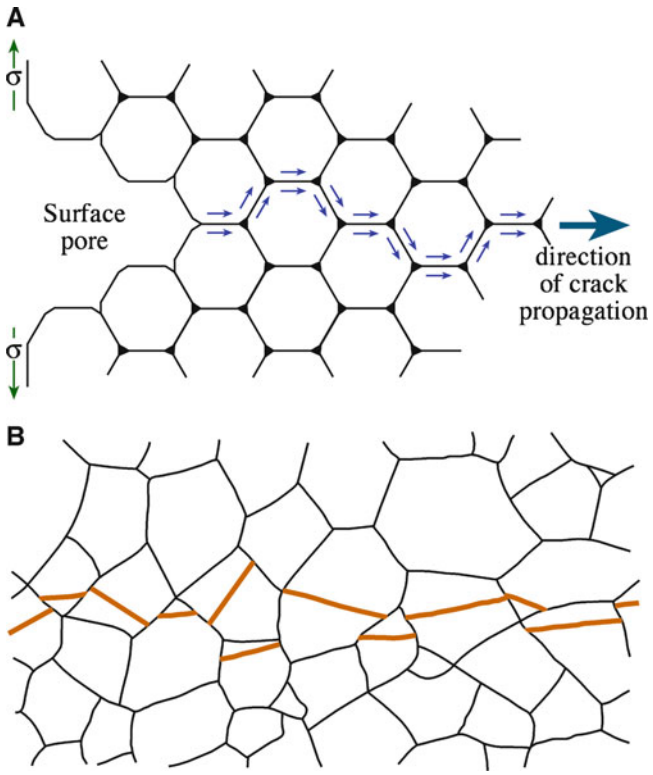

FIGURE 18.12. (A) Intergranular cracking. (B) Transgranular cracking.

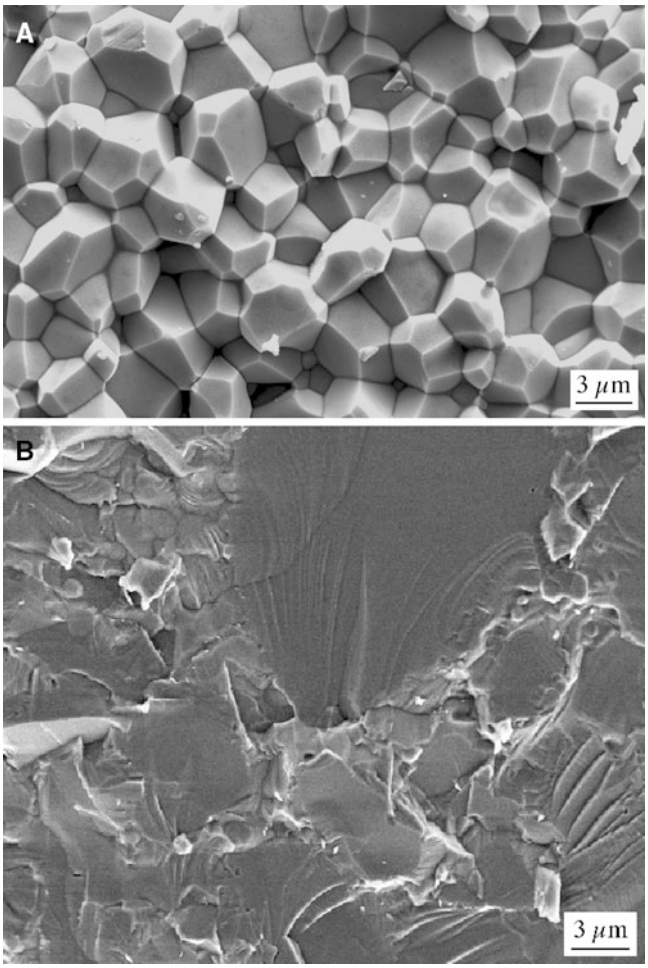

FIGURE 18.13. (A) Fracture surface of polycrystalline AlN. (B) Fracture surface of polycrystalline SiC.

In glasses it is often quite easy to determine the origin of fracture, as shown in Figure 18.15. We can identify three distinct regions on the fracture surface.

Mirror—The region around the crack origin. The crack travels in a single plane, accelerating as it goes. The fracture surface is smooth and highly reflective. It can

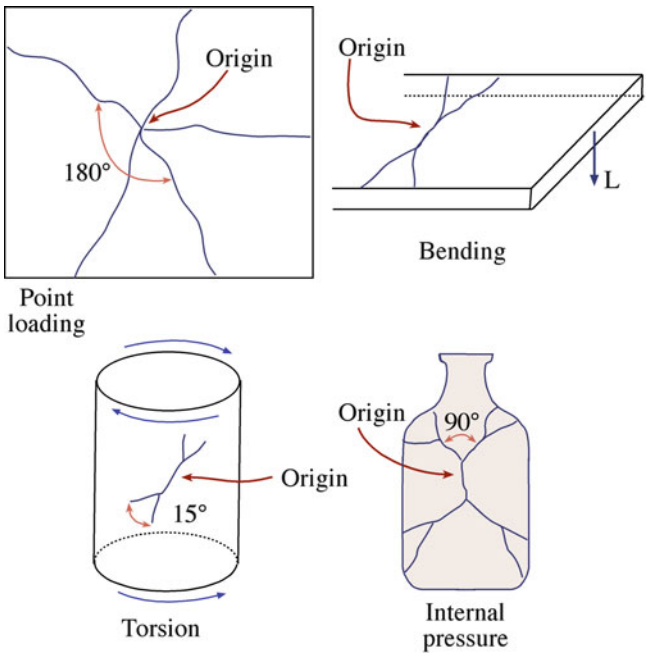

FIGURE 18.14. Determination of crack origin and failure mechanism by postmortem examination of glass fragments.

be seen in polycrystalline ceramics, but reflectivity is lower.

Mist—The crack deviates because it reaches a critical velocity, intersects an inclusion, or there is a change in the internal stresses in the glass. The fracture surface is rougher and less reflective. This region is often difficult to see in polycrystalline ceramics.

Hackle—Crack branches form larger ridges and further increase the roughness of the fracture surface. By tracing the hackle lines backward, we can usually determine the origin of fracture.

Hackle is also referred to as river patterns because of the similar appearance to a river branching into tributaries. Figure 18.16 illustrates river patterns on the fracture surface of an Nd-doped YAG single crystal that fractured during growth. The irregular-shaped voids seen in the image are where failure originated.

18.9 TOUGHENING AND CERAMIC MATRIX COMPOSITES

Ceramics usually have low fracture toughness. For many engineering applications, we must increase the toughness. The desire to toughen ceramics is not new. Toughening of brick using straw was known in 9,000 BCE. The basic idea is how to stop crack movement, thereby increasing the amount of energy required for crack propagation.

TOUGHENING
We want to increase G_c to toughen the ceramic.

The toughening mechanisms for ceramics are summarized in Table 18.6. A stress–strain curve for a toughened ceramic is shown in Figure 18.17. In this particular case, reinforcing the ceramic matrix—a lithium aluminosilicate (LAS) glass ceramic—with fibers (SiC) produced the desired toughening. The resulting fracture surface is shown in Figure 18.18. Toughening is achieved by bridging of the crack surfaces behind the crack tip by a strong reinforcing phase. The stress intensity at the crack tip is reduced, and this slows crack propagation. The fibers absorb energy as the crack front advances. An additional energy-absorbing process that often accompanies crack bridging is fiber pullout away from the crack plane, as illustrated in Figure 18.19.

The factors that contribute to the fracture toughness of a composite are:

- Volume fraction of reinforcement. Figure 18.20 shows how fracture toughness increases for SiC whisker-reinforced ceramics as a function of increasing whisker content.
- Young's modulus of matrix and reinforcement. If a matrix is reinforced with high-modulus, high-strength fibers, then more of the stress can be carried by the fibers.
- Strength of the matrix/reinforcement interface. In fiber-reinforced composites, a strong interface can lead to transfer of the stress from matrix to the fibers; a weak interface can lead to debonding and crack deflection.

For the specific case where toughening is due to elastic deformation of a partially debonded reinforcement with no interfacial friction, K_{IC} has been determined to be:

$$K_{Ic} = \sqrt{\{\mathcal{E}_c G_m + \sigma_f^2[(rV_f\mathcal{E}_c\gamma_f)/(12\mathcal{E}_f\gamma_i)]\}} \quad (18.23)$$

The subscripts c, m, and f refer to the composite, matrix, and reinforcement, respectively. Increases in fracture toughness are predicted by:

- Increasing V_f
- Increasing $\mathcal{E}_c/\mathcal{E}_f$
- Increasing γ_f/γ_i

The last item in the list implies that toughness is enhanced when the interface between the fiber and matrix is weak. The crack then passes around the fiber, as shown in Figure 18.21.

An important toughening mechanism involves a phase transformation in zirconia (ZrO_2). The best-known example is zirconia-toughened alumina (ZTA), which contains 10–20 vol% of fine ZrO_2 particles. At elevated

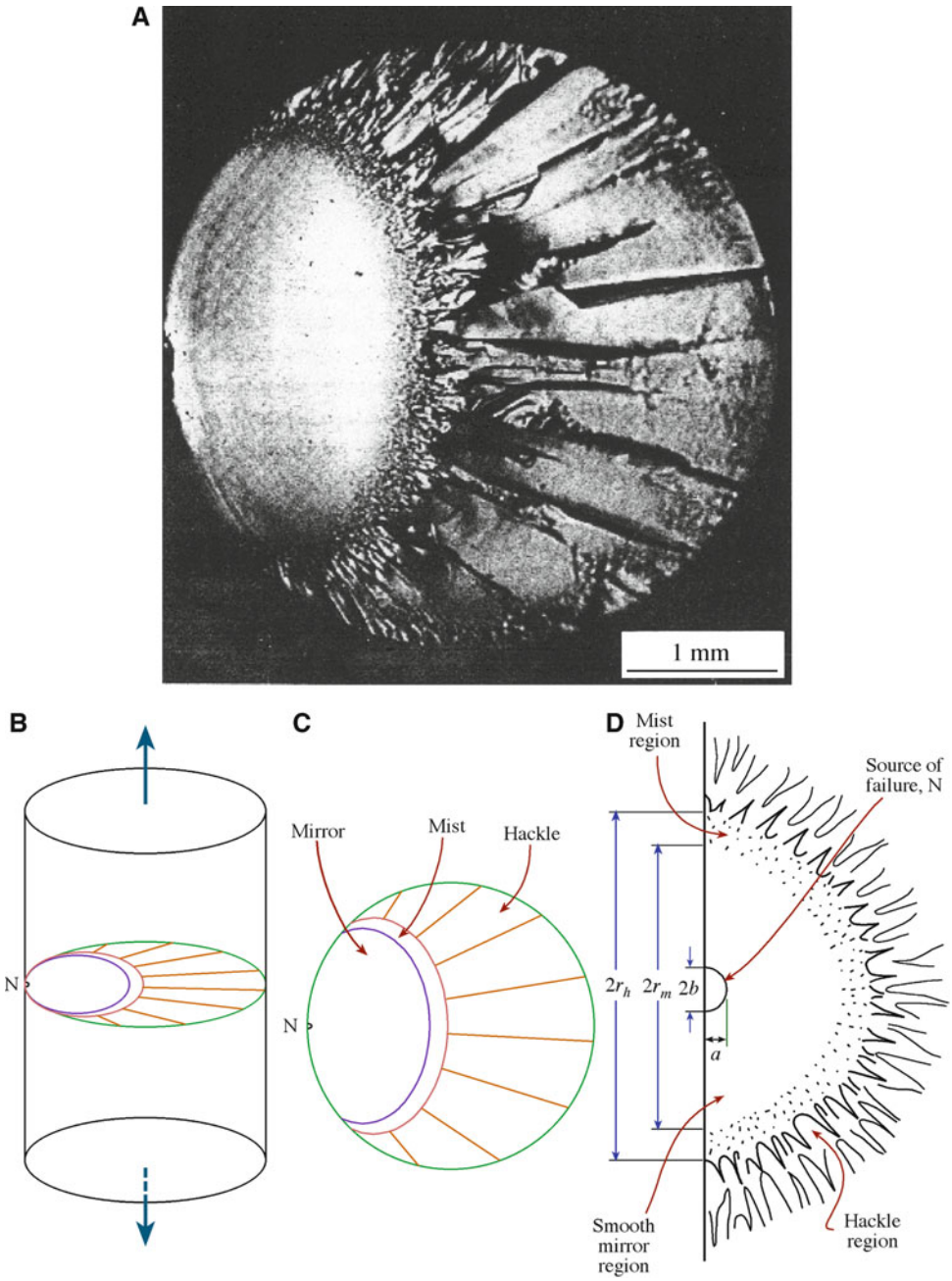

FIGURE 18.15. Fracture surface of a glass rod and corresponding schematics illustrating the distinct regions of the surface.

temperatures the equilibrium structure of ZrO_2 is tetragonal (t), and at low temperatures it is monoclinic (m). On cooling ZTA from the high temperatures required for fabrication, t → m transformation may occur in the zirconia particles. This transformation is accompanied by an increase in volume of about 3%.

The transformation is athermal; that is, it is not time-dependent and proceeds very rapidly. If the transformation takes place in the ZrO_2 particles during fabrication of ZTA ceramics, then the 3% volume change produces stresses in the alumina matrix around the transformed particle, leading to microcracking. These microcracks increase the toughness of the ceramic because of their ability to deflect and bifurcate a propagating crack. Control of the extent of the microcracking determines the increase in toughness. The optimum conditions are when the particles are large enough to transform but only small enough to cause limited microcrack development. If microcracking becomes extensive, the cracks can interact, resulting in a decrease in strength. Zirconia particle size is controlled by:

- Milling prior to sintering
- Aging after sintering

If a stabilizing oxide (e.g., 3 mol% Y_2O_3) is added to the zirconia, then it is possible to suppress the t → m

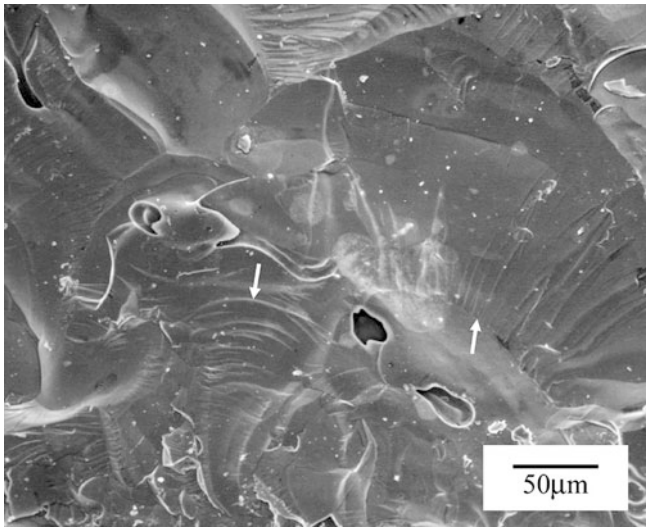

FIGURE 18.16. Scanning electron microscopy (SEM) of the fracture surface of Nd-doped YAG. River marks are indicated by arrows.

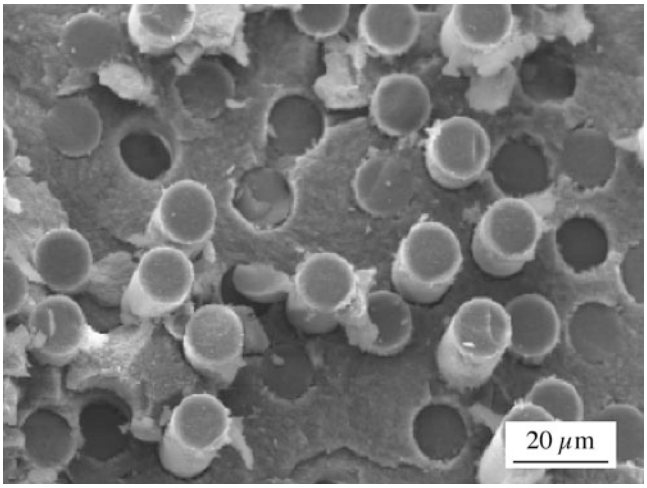

FIGURE 18.18. SEM image shows fiber pullout on the fracture surface of $AlPO_4$-coated alumina/mullite fiber/Al_2O_3 CMC, hot pressed at 1,250°C for 1 h.

TABLE 18.6 Classification of Toughening Mechanisms in Ceramics

General mechanism	*Detailed mechanisms*
Crack deflection	Tilt and twist out of crack plane around grains and second-phase additions
Crack bowing	Bowing in crack plane between second-phase crack-pinning points
Crack branching	Crack may subdivide into two or more roughly parallel cracks
Crack tip shielding by process zone activity	Microcracking
	Transformation toughening
	Ductile yielding in process zone
Crack tip shielding by crack bridging	Second-phase brittle fibers with partial debonding
	Frictional and ligamentary grain bridges
	Second-phase ductile ligament bridging

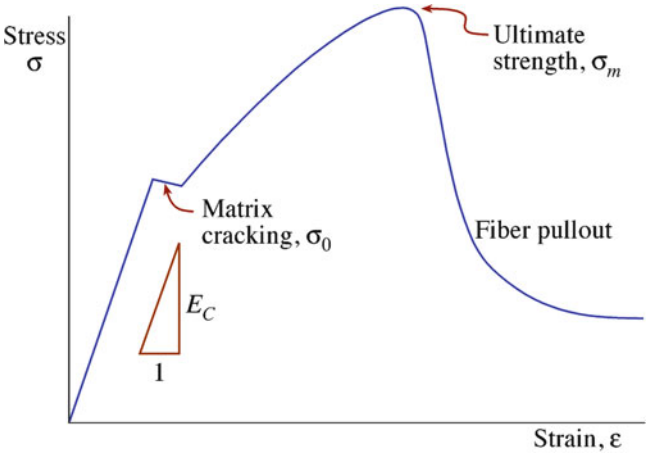

FIGURE 18.17. Stress–strain curve for a tough fiber-reinforced ceramic matrix composite.

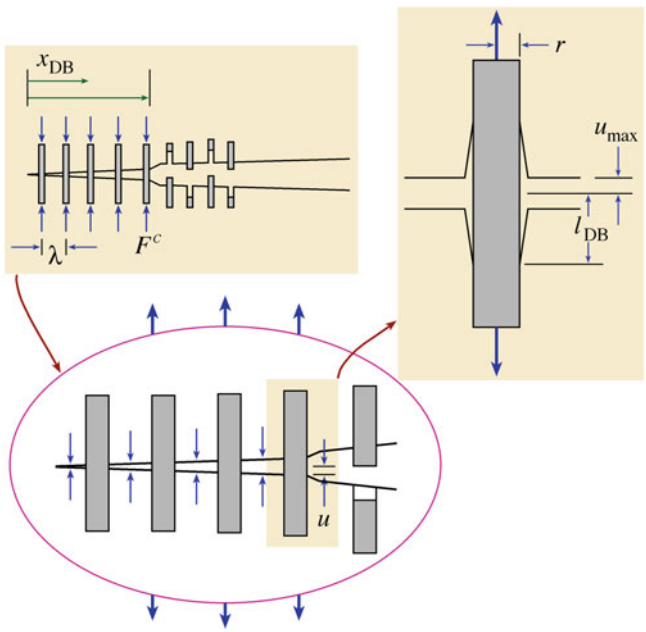

FIGURE 18.19. Crack bridging mechanism with debonding and fiber pullout.

transformation on cooling from the fabrication temperature. The ZrO_2 particles can be retained in the metastable tetragonal form at room temperature. Whether the transformation takes place or not depends on the amount of stabilizing oxide and the particle size. The presence of the alumina matrix makes it difficult for the volume expansion associated with the transformation to be accommodated. The constraint is such that small particles are less likely to transform than large particles. With a suitable combination of the amount of stabilizing oxide and particle size, it is possible to obtain a dispersion of metastable tetragonal particles.

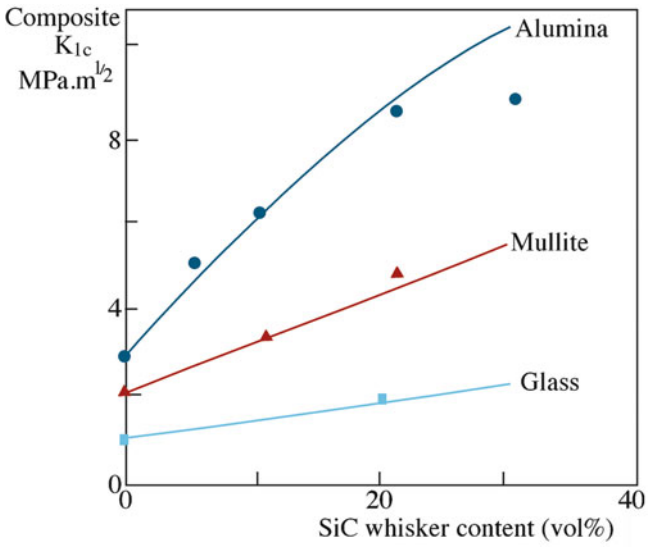

FIGURE 18.20. Effect of SiC whisker content on toughness enhancement in different matrices.

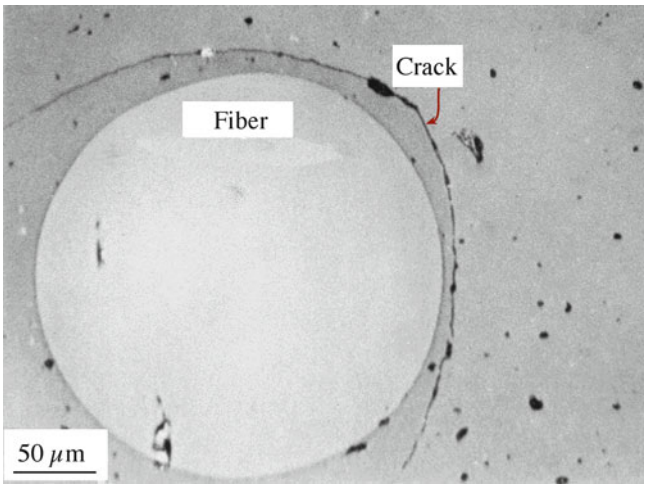

FIGURE 18.21. SEM shows crack propagation around a sapphikon (Al_2O_3) fiber in a calcium aluminosilicate (CAS) glass-ceramic.

Under the influence of the stress field at a crack tip, these particles transform athermally to the monoclinic state. This leads to transformation toughening. The toughening increment ΔK_T that can be achieved by this mechanism is:

$$\Delta K_T = A V_{ZrO_2} \varepsilon_T \mathcal{E}_m w^{1/2} \tag{18.24}$$

where A is a constant with a value close to unity, V_{zirc} is the volume fraction of the metastable particles, ε_T is the volume strain accompanying the transformation, $\mathcal{E}_m$ is Young's modulus of the matrix (often alumina), and w is the width of the process zone around a crack containing transformed particles (shown in Figure 18.22).

It is important to note that, in contrast to ZTA toughened by microcracking, transformation toughening can lead to an improvement in both toughness and strength and consequently is the preferred toughening mechanism.

The effectiveness of the different toughening mechanisms for structural ceramics appears to decrease in the following order.

- Continuous fiber reinforcement (most effective)
- Metal dispersed particles
- Transformation toughening
- Whiskers/platelet/particle reinforcement
- Microcracking (least effective)

Some examples and associated toughness values are given in Table 18.7. It is worth remembering that although the values are higher—in some cases by an order of magnitude—than for single-phase polycrystalline ceramics they are still much lower than most engineering metal alloys.

18.10 MACHINABLE GLASS-CERAMICS

Machinable glass-ceramics (MGCs) rely on controlled fracture. In Macor®, a commercial MGC made by Corning, the crystalline phase is fluorophlogopite mica.

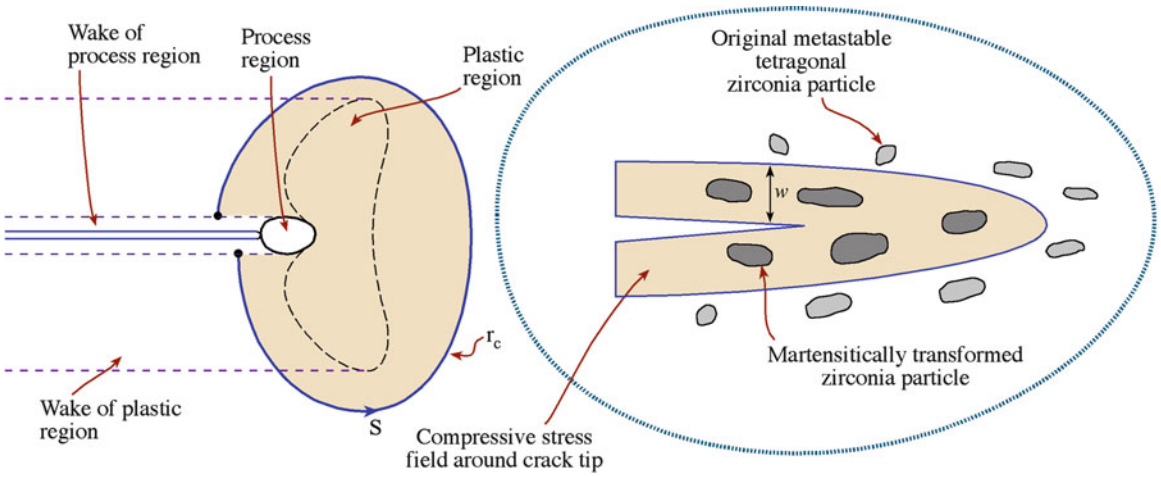

FIGURE 18.22. Transformation toughening in a ceramic matrix containing ZrO_2 particles.

TABLE 18.7 Effects of Different Toughening Mechanisms

Mechanism	*Highest value achieved (MPa/m^2)*	*Exemplary systems*
Continuous fiber reinforced	>30	SiC-SiC; Glass-SiC
	>25	Glass-ceramics-SiC
	~16	Si_3N_4-SiC
Metal dispersed	~25	Al_2O_3-Al; Al_2O_3-Ni
Transformation	~20	ZrO_2 (MgO)
Platelet	~14	Si_3N_4-SiC
Whisker	~11	Si_3N_4-SiC
	~8.5	Al_2O_3-SiC
Particle	~8	Si_3N_4-SiC
Microcracking	~10	Al_2O_3-ZrO_2

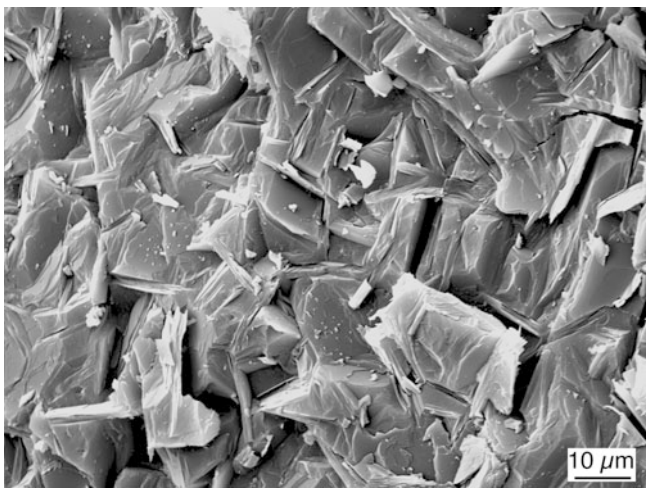

FIGURE 18.23. Fracture surface of Macor®.

The mica forms as randomly oriented grains in a borosilicate glass matrix. During machining, cracks propagate along the glass/mica interface (intergranular), and material is removed. Figure 18.23 shows the fracture surface of Macor® where the mica crystals, which look like packs of cards, can be clearly seen. MGCs can be machined using either high-speed steel or tungsten carbide cutting tools. They can be used at high temperatures (up to 1,000°C); and because of their high chemical resistance, they are used for precision valves and nozzles in the chemical industry. Table 18.8 lists the composition of Macor® and some of its properties.

18.11 WEAR

Wear resistance is the ability of a material to resist mechanical (or chemical–mechanical) abrasion. There are two main mechanisms that lead to removal of material from the surface of a ceramic.

TABLE 18.8 Composition (wt%) and Properties of Macor®, a machinable glass-ceramic

SiO_2	Al_2O_3	B_2O_3	K_2O	MgO	F
46	16	7	10	17	4

Property	*Value*
Coefficient of thermal expansion (ppm/°C)	7.4–12.6
Thermal conductivity ($W\ m^{-1}\ °C^{-1}$)	1.46
Continuous operating temperature (°C)	800
Maximum no-load temperature (°C)	1,000
Density (g/cm^3)	2.52
Young's modulus at 25°C (GPa)	66.9
Poisson's ratio	0.29
Shear modulus at 25°C (GPa)	25.5
Knoop hardness, 100-g load	250
Modulus of rupture at 25°C (MPa)	94
Compressive strength (MPa)	345
Fracture toughness (MPa/m^2)	1.53

TABLE 18.9 Erosion Resistance versus Hardness for Several Ceramics

Material (in order of increasing erosion resistance)	*Knoop hardness (kg/mm^2)*
MgO	370
SiO_2	820
ZrO_2	1,160
Al_2O_3	2,000
Si_3N_4	2,200
SiC	2,700
B_4C	3,500
Diamond	7,000–8,000

- Grain pullout—In polycrystalline ceramics with weak grain boundaries
- Cracking—Fracture due to abrasion, gouging, or erosion

Wear resistance is usually closely associated with hardness and corrosion resistance. For example, Table 18.9 shows how erosion resistance correlates directly with hardness. Erosion usually specifies wear of a material by an abrasive in a fluid, the type of situation encountered when ceramics are polished.

Although ceramics are generally characterized as being wear-resistant, their commercial use as wear parts is less than 10% of the overall market.

Alumina is the most commonly used wear-resistant ceramic. One of the early applications was in seal faces for rotary water pumps for automobiles. Alumina is particularly suitable because it is resistant to engine cooling fluids. Another application for alumina, which we mentioned in Chapter 16, is in total hip prostheses. In terms of wear rates at the contact surfaces between the ball and socket, alumina is far superior to the alternative metal and polymer systems.

Alumina and toughened zirconia ceramics are used in the wire drawing industry as capstans, pullets, and guides. Improved product quality, longer component service life, and lower manufacturing costs have been attributed to the use of ceramics. For example, ceramic capstans last up to 10 times longer than carbide-coated capstans.

As with other mechanical properties, there are standard tests to measure wear resistance. The main method is described in ASTM G99, which uses a pin-on-disk apparatus. This test is used to measure sliding wear of ceramics and ceramic coatings.

18.12 GRINDING AND POLISHING

Grinding and polishing both use controlled fracture. Abrasives are the basis of an important ceramic industry. For example, the abrasive used in Emory paper is SiC; sandpaper uses SiO_2. The historically important abrasive was jeweler's rouge (hematite). Now, ceria (CeO_2) is often preferred for glass and ceramics, and colloidal silica (e.g., Syton™) is used for Si. Abrasive particles are almost always ceramics (usually oxides, carbides, or diamond). The polishing action actually involves an interaction between two surfaces, with the second surface being that of the abrasive particle. Figure 18.24 illustrates mechanical polishing using abrasive grains held in a soft pad. Table 18.10 lists some of the common abrasives used for polishing ceramics together with their hardness.

The abrasive is often applied as slurry onto a soft pad. A series of polishing steps are used, with abrasives of decreasing particle size (eventually down to as small as 4 nm). The final step produces a smooth specular surface, which is good enough for film deposition.

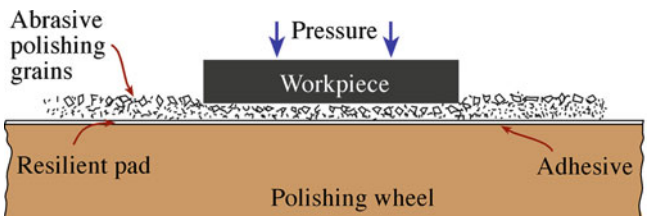

FIGURE 18.24. Polishing process using abrasive grains held in a soft pad. This method is the one most often used in university metallography laboratories.

TABLE 18.10 Hardness of Selected Abrasives Used in the Polishing of Ceramics

Abrasive	*Mohs hardness*	*Knoop hardness*
Zirconia	8	1,160
Garnet	8	1,360
Calcined alumina	9	2,100
Silicon carbide	9–10	2,480
Boron carbide	9–10	2,750
Cubic boron nitride	10	4,500
Diamond	10	7,000

Chemical/mechanical polishing (CMP) may also be used. In this case, an abrasive is used together with a chemical (usually either an acid or a caustic solution) that produces an etching action. CMP is actually very complex and still not fully understood. Final CMP may involve an abrasive that is softer than the materials being polished.

An example of a modern commercial polishing cloth is shown in Figure 18.25. The pyramids are particles of ceria bound in a polymer on a flexible cloth. This type of fixed abrasive has the advantage over a slurry in that the abrasive is well controlled and can be easily changed/renewed and that there is always a clear channel for the electrolyte to reach the polishing site.

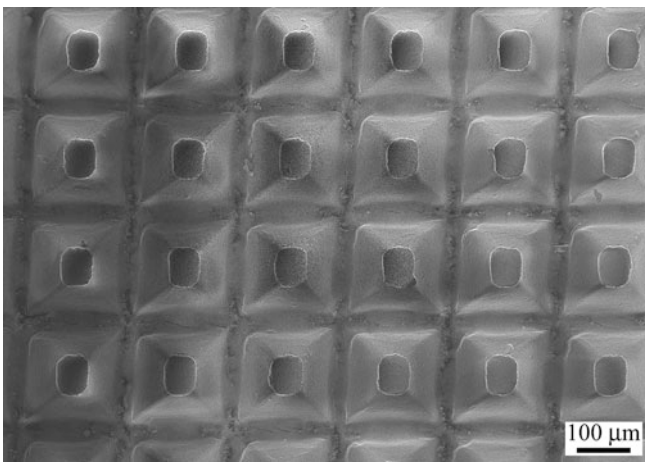

FIGURE 18.25. SEM of ceria particles in a modern polishing cloth.

CHAPTER SUMMARY

Although we often think of the brittleness of ceramics as a distinct disadvantage, the very existence of our civilization depended on this property. We make use of brittleness in many applications, such as in sculptures and for polishing; but for reliable structural uses, we often need better fracture toughness. One way to achieve this is to form a composite by adding some fibers to a ceramic matrix. The fibers provide additional mechanisms for energy absorption during fracture. The key work in understanding brittle fracture goes back to that of Griffith.

(continued)

CHAPTER SUMMARY (*continued*)

He showed that flaws act as stress concentrators, which lead to measured strengths—significantly, those predicted by theory. The work of Griffith is the link to the Weibull statistics we described in Chapter 16. By examining fracture surfaces, a process called "fractography," we can often determine how and why a brittle material failed. This information can be useful in guiding processing methods to avoid stress concentrators, such as porosity and inclusions.

PEOPLE AND HISTORY

Griffith, Alan Arnold (1893–1963), known as "the father of fracture mechanics" and "bubble Griffith"—the first for his classic work in fracture mechanics and the role of flaws, the second for his work on soap films. He was a British aeronautical engineer who worked at Rolls-Royce from 1939 to 1960 designing turbojet engines.

Inglis, Sir Charles Edward (1875–1952) was professor of engineering at Cambridge University. He was best known for his work on stress in metal plates when cracks are present.

Orowan, Egon (1901–1989) was born in Budapest, Hungary and died in Cambridge, Massachusetts. In addition to his work on fracture, he showed the importance of the dislocation in plastic deformation. He joined MIT as a professor in 1950.

EXERCISES

18.1 Carbon nanotubes have been proposed as a material for the next generation of ceramic armor. (1) What are the properties of carbon nanotubes that make them of interest for this application? (2) Are there practical limitations that currently prevent their widespread use?

18.2 Calculate the theoretical strength of MgO. Are there any conditions under which this value would be attainable?

18.3 A sharp notch 0.1 mm long is introduced into the surface of a fused silica plate. The plate is then loaded to 100 MPa in tension normal to the notch. (a) Does the plate fracture? (b) If not, what is the applied stress that would lead to fracture? (c) If the plate was made of a lithium-aluminum-silicate (LAS) glass-ceramic, what applied stress would lead to fracture?

18.4 A soda-lime silica plate failed at 100 MPa. (1) Estimate the flaw size and state any assumptions you make. (2) If the plate were made of fused silica and contained the same flaw size, what is the maximum applied stress it could withstand without breaking? Assume the glass has $\mathcal{E} = 70$ GPa.

18.5 A manufacturer of silicon nitride jet engine parts found that a recent batch of samples became damaged during processing and had surface flaws about 50 m deep. The normal average flaw size in these parts is about 10 m. (1) Estimate the tensile strength of these samples. (2) Estimate the compressive strength of these samples.

Ceramic	Maximum flaw size (μm)	Average flaw size (μm)
Si_3N_4	20	15
SiC	30	18
MgO	10	7
Al_2O_3	5	3

18.6 You have been hired as a consultant and asked to choose the best ceramic for a load-bearing application. A vendor has offered you the following options. Which one would you take and why? Are there any other factors that you need to consider before you make your final recommendation?

18.7 In Table 18.6, we list different toughening mechanisms for ceramic–matrix composites (CMCs). Illustrate each mechanism using a sketch and, where appropriate, indicate the differences between using particles, platelets, and fibers as the reinforcement.

18.8 Explain how the addition of zirconia particles can lead to toughening of a ceramic. Suggest other additions that might produce similar toughening effects.

18.9 Draw sketches similar to Figure 18.10 to indicate how (1) ammonia and (2) methanol might lead to stress corrosion cracking in glass.

18.10 Figure 18.13A shows the fracture surface of polycrystalline AlN. Can you see any evidence of transgranular failure?

18.11 Explain why we can write equation 18.1.

18.12 Using the values in Table 18.2, discuss the theoretical strength of MgO and NaCl. Do these values seem sensible, and why are they so different?

18.13 Explain how Figure 18.3 is related to Weibull statistics.

18.14 In deriving equation 18.12, we say it assumes an atomically sharp crack. How does this assumption affect the formula, and is it reasonable for an MgO?

18.15 Why does Figure 18.6 verify equation 18.12? What information can you deduce from such a graph?

18.16 Using Table 18.4, discuss and compare K1c for (1) both forms of zirconia; (2) MgO and KCl; (3) CaF_2 and ThO_2; (4) LAS and silica glass.

18.17 Why are equations 18.17 and 18.18 different? How does this affect our use of ceramics?

18.18 Explain to a metallurgist what Figure 18.9 is showing.

18.19 Explain how Figures 18.10 and 18.22 are related.

18.20 What value of toughness do we need for ceramic armor?

GENERAL REFERENCES

Green DJ (1998) An introduction to the mechanical properties of ceramics. Cambridge University Press, Cambridge, UK

Hull D (1999) Fractography. Cambridge University Press, Cambridge, UK

Lawn B (1993) Fracture of brittle solids, 2nd edn. Cambridge University Press, Cambridge. UK

Tabor D (2000) The hardness of metals. Oxford University Press, Oxford, UK, Reprint of the 1959 classic. Very readable

SPECIFIC REFERENCES

Garvie R, Hannick RHJ, Pascoe R (1975) Ceramic steel? Nature 258:703, First description of transformation toughening

Griffith AA (1920) The phenomenon of rupture and flow in solids. Phil Trans R Soc Lond A221: 163–98. (1924) The Theory of Rupture. In: Biezeno CB, Burgers JM (eds) Proceedings of 1st international congress applied mechanics. p 55

Inglis CE (1913) Stresses in a plate due to the presence of cracks and sharp corners. Trans Inst Nav Archit A127:219–230, he Inglis equation (Eqn. 18.13)

Johnson JW, Holloway DG (1966) On the shape and size of the fracture zones on glass fracture surfaces. Philos Mag 14: 731–743. Also Microstructure of the mist zone on glass fracture surfaces. Philos Mag 17: 899–910

Obreimoff JW (1930) The splitting strength of mica. Proc R Soc Lond A127:290–97, Early study of the fracture of mica (Section 18.3)

Orowan E (1949) Fracture and strength of solids. Rep Prog Phys 12:185–232